Journal of Materials Science Research; Vol. 12, No. 2; 2023
ISSN 1927-0585 E-ISSN 1927-0593
Published by Canadian Center of Science and Education

Correlation of Accelerated Corrosion and Real Reinforced Concrete Water Structures

Philip Mogire[1]

[1] Department of Civil Engineering, South Eastern Kenya University, Kitui, Kenya

Correspondence: Philip Mogire, Department of Civil, Construction and Environmental Engineering, South Eastern Kenya University, 170,90200, Kitui, Kenya. E-mail: philosiemo@yahoo.com

Received: June 20, 20233 Accepted: July 28, 2023 Online Published: August 15, 2023

doi:10.5539/jmsr.v12n2p88 URL: https://doi.org/10.5539/jmsr.v12n2p88

Abstract

The service life of reinforced concrete constitutes the initiation and propagation period. Accelerated corrosion tests are carried out to obtain results in modelling the Service life of reinforced concrete structures. Its erroneous to undertake a direct linear extrapolation of accelerated test results to real structures in predicting their service life. This research examines the relationship between the result from accelerated corrosion and real reinforced concrete water structures. The physical and chemical properties of the materials used in the study were investigated for compliance for use in reinforced concrete water structures. Concrete of three classes M25, M30 and M35 were used to cast accelerated corrosion test samples. For each class 9 concrete samples of diameter 100 mm, 130 mm and 150mm respectively and 300mm long were prepared. A 10 mm diameter bar, 400 mm long was centrally inserted during casting. After curing the test samples were immersed in a 3.5% solution of sodium chloride solution under 6 V. The accelerated corrosion specimens were monitored for onset of cracks and stopped when the cracks were 0.2 mm in width. Using the accelerated corrosion and real reinforced concrete results, a parametric study of the propagation period was done and a model proposed. From the results the proposed and published propagation period model compares well. The result from accelerated corrosion and real reinforced concrete water structures lineally increase for the propagation period. The proposed model can be considered as an input parameter for the service life of actual reinforced concrete water structures and contribute to their optimum performance.

Keywords: Service Life model, Corrosion, Real Reinforced Concrete Structures.

1. Introduction

Reinforced concrete deterioration due to corrosion resulting from chloride ingress or carbonation plays a significant role in reduction of the design service life of reinforced concrete water structures attracting researchers of various disciplines during the past three decades (Hossein, Keivan, & Hashemian). Metals release the potential energy during the corrosion process after reacting with the favorable corrosive species. The metals then revert to compounds more or less similar to their original states. The energy stored during melting and released during corrosion supplies the driving potential for the corrosion process to take place (Palanisamy, 2019). Corrosion occurs when at least two metals (or two locations of the reinforcing bar) is at different energy levels. In reinforced concrete the concrete acts as an electrolyte while the rebar act as a metallic connection (Palanisamy, 2019). At a pH of 12–13, reinforced concrete is in an alkaline state and a thin oxide layer forms on the steel and prevents metal atoms from dissolving forming a passive film (Ghods, 2012). The passive film reduces the corrosion rate to an insignificant level without which the steel would corrode at rates at least 1,000 times higher (ACI 222R-01).

The presence of rust on reinforcement bars and appearance of cracks parallel to the reinforcement bars is an indication of corrosion in reinforced concrete structures. The main causes of electrochemical corrosion in reinforced concrete is carbonation and chlorides which induces a generalized attack and localized attack respectively. Carbonation induced corrosion commonly occurs in relatively dry environments where sufficient carbon oxide diffuses through the concrete cover. In chloride containing environments, the chloride ingress is usually faster than the carbonation process, and it is more likely to be the predominant cause of deterioration in reinforced concrete water structures by degrading the resistance of the structure to service load.

A number of corrosion models have been proposed; broadly categorized into either empirical (Alonso, 1998), analytical (Pasant, 1979; Liu, 1998) or numerical (Li, 2006; Molina, 1993). Molina used a smeared crack model for the finite element analysis of cover cracking due to reinforcement corrosion. In their model they presumed

corrosion of steel to take a linear variation of the material properties from those of steel to those of rust. They assumed that the mechanical properties of rust nearly resemble that of water, one of the main constituents of rust. Their analysis was based on the experiments of Andrade, 1993, where the thickness of the concrete cover was 1.25 and 1.9 times the reinforcement diameter.

Morinaga (1989) suggested an empirical equation for predicting the time to cover cracking without reference to the evolution of the damage zone. In his empirical equation; the time to cover cracking was taken as a function of the corrosion rate, concrete cover thickness and reinforcing diameter. The results predicted by this model is much shorter than the experimentally observed values (Morinaga, 1989; Liu, 1998).

Further investigations in this field have revealed that the consideration of the appropriate mechanical behavior of corrosion products strongly affects the predicted results (Bhargava, 2006). Lundgren (Lundgren, 2002), in an effort to study rebar pull-out, presented a reasonable way to model the effect of corrosion on the bond between the corroded reinforcement and concrete. Lundgren employed finite element analysis and assumed that rust behaves like granular materials, in accordance with the experimental tests of Andrade (Andrade, 1993). Lundgren pointed out that the model could predict the decrease of the bond when splitting of the concrete occurs. It was emphasized that axisymmetric analysis appears to be a satisfactory level of modeling when a study of concrete cover cracking due to uniform corrosion is of concern. However, three dimensional models should be used if localized corrosion is to be studied.

Bhargava et al., 2006, presented a mathematical model to predict the time to concrete cover cracking and weight loss of reinforcing bars. However, they assumed that the mechanical properties of corrosion products are the same as those of steel, although reasonably good agreement was obtained between experimental results and the analytical predictions. They showed that tensile strength, initial tangent modulus of concrete, annual mean corrosion rate, and modulus of elasticity of the reinforcement and corrosion significantly influence the predicted time to cover cracking.

In this study a mathematical model is formulated to determine the corrosion rate in water structures. This model takes into consideration of the serviceability limiting condition of the crack width of water structures.

2. Methodology

The study was conducted at the University of Nairobi Concrete and Materials Lab, where the physical properties of the materials were identified and the sample preparation and testing were done. The chemical properties of the selected Cem 1 brands were identified in the State Department of Infrastructure in the Ministry of Transport, Infrastructure, Housing and Urban Development of the Government of Kenya.

2.1 Cement, Aggregates and Water for the Study

Available Cem 1 brands of cement in Kenya are manufactured in accordance with (KS EAS 18-1:2017). The cements were sourced from a local wholesaler and were randomly selected. Table 1 shows the sources of the fine aggregate (FA), coarse aggregates (CA) reinforcing steel bar and water used in this study.

Table 1. Details of material for this study

SN	Description	Source	Remark
1.	Fine aggregates	Machakos River	
2.	Coarse aggregates	Kenya Builders quarry	5-20mm graded at source
3.	10mm ribbed bars	Local Manufacturer	Factory cut to 1010mm length
4.	Mixing water	lab	Portable

2.2 Test for Mechanical Properties of Aggregates

Table 2 shows the reference standard used for the procedure of testing aggregates the physical and mechanical properties of aggregates.

Table 2. Testing procedure for physical and mechanical properties of aggregates

Test	Standard for test procedure
Specific gravity	ASTM C128
Water absorption	BS 812-2:1995
Silt content	ASTM C142-97
Crushing value	BS EN 1097-2
Impact value	BS EN 1097-2
Flakiness index	BS/EN 933-3
Los Angeles abrasion value	BS/EN 1097-2

2.3 Mix Design

The concrete used for this study was of characteristic strength 25 N/mm^2, 30 N/mm^2 and 35 N/mm^2 designed according to the Department of Environment's Design (DOE) method (Ejiogu, 2020) and constituted the proportions shown in Table 3.

Table 3. mix proportions of materials for this study

Characteristic strength (N/mm^2)	Coarse aggregates (kg/ m^3)	Fine aggregates (kg/ m^3)	Cement (kg/ m^3)	Water(kg/m^3)
25	1190	650	450	225
30	1069	638	450	225
35	1075	631	469	225

Using the mix proportions, fresh concrete was prepared by using an electric mixing pan, poured into the moulds in five layers and vibrated by a vibrating table for 60 seconds. A slump test was carried out for each batch of concrete. After 24 hours, the moulds were removed and the concrete specimens cured at normal room temperature in a water tank for 27 days.

2.4 Sample Size and Precision

Cubes of size 150mm*150mm*150mm, cylinders with a diameter of 150mm*300mm long, cylinders of diameter 150mm*30mm long with 10mm diameter*1010mm long reinforcing ribbed steel bar centrally placed were pepared in line with BS 12390-1:2012, BS EN 12390-5:2009 and ACI 318 -08 specifications for compressive strength, tensile strength and bond strength tests. A total number of 27 cubes, 27 cylinder specimens for tensile strength and 27 cylinders for bond strength were prepared, cured and tested according to the methods stipulated in BS EN 12390-2:2019, BS EN 12390-6:2009, for 7,14 and 28 days' compressive strength, tensile and bond strength. Each sample for compressive strength was subjected to loading until failure using an automated electronic testing machine, which conforms to BS EN 12390-4:2019. A universal testing machine (UTM) maximum load of 2000 kN was used to test the cylinders for tensile strength.

The bond strength study was carried out through a pull out test in which a manually operated hydraulic pump with a load cell of 100 kN was used. The load was applied at a rate of 2 kN/sec and distributed on the specimen surface by a 200 mm square steel plate with a hole at the center system. The setup of the pull out test is shown in Figure 1.

(a) Sample confining apparatus

(b) Tensile load detection equipment

Figure 1. (a)- (b) Pull out Testing equipment during sample testing (Source: Author)

Bond stress (S) in MPa was calculated as average stress between the reinforcing bar and the surrounding concrete along the embedded length of the bar from Equation 1.

$$S = \frac{P_{max}}{\pi d_b L_d} \quad (1)$$

Where P_{max} was the maximum pullout load(N)), d_b was diameter of the bar(mm) and L_d was the embedded bar length(mm).

2.5 The Accelerated Corrosion Test

2.5.1 Materials and Specimens

This was done through an impressed corrosion test using the procedure below;

i) 10 mm diameter x 400 mm long ribbed bars were polished with abrasive papers.

ii) 120 mm of the surface length of each bar were sprayed with a zinc rich coating and left to naturally dry.

iii) The mixed concrete (in two batches) was poured into 9 cylindrical samples of 150 mm diameter and 30 0mm long, 130 mm diameter and 300 mm long, 100 mm diameter and 300 mm long each with a 10 mm diameter rebar

iv) The specimens were mechanically vibrated for 60 s. After 24 hours, the cylindrical concrete specimens were demolded and cured for 27 days.

v) The test specimens were dried for 24 hours and then subjected to accelerated corrosion by storing them in a tank containing 3.5 % NaCl at room temperature and an impressed voltage of 6volts applied through a DC power supply regulator. The top and bottom surfaces of the concrete specimens were also sealed with Zinc rich coating so as to allow chloride ingress from the sides to simulate the corrosion of a section of a typical structural member in a water conveyancing structure.

2.5.2 Testing Methodology

The accelerated corrosion set up is shown in Figure 2. The rebars projecting were connected in series to the anode and the stainless steel rod was connected to the negative terminal (cathode). The test specimens were subjected to a constant voltage of 6 V applied to the system using a DC power supply regulator. The variation in development of corrosion current was monitored at regular intervals using a high impedance multitimeter and the average for the corrosion period taken for calculation of the average mass loss.

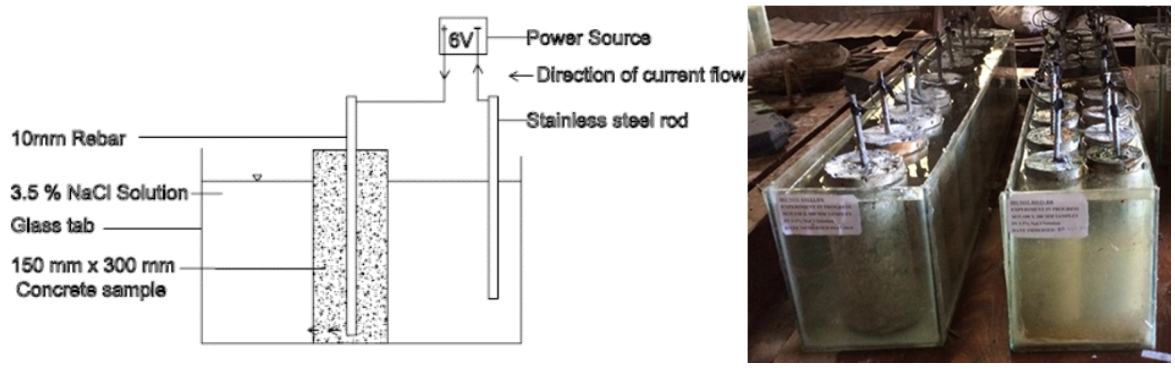

a) b)

Figure 2. a) Schematic drawing of accelerated corrosion set up, b) Photo of the samples during experimentation

The appearances of first visible cracking were detected by visual observation using a magnification glass with power of x1000. The data collected for crack propagation provided the timing of first cracking and the subsequent time-dependent increase in crack width. After testing, the weight loss of bars due to corrosion were studied by cleaning, drying and weighing the reinforcement bars according to the gravimetric weight loss method as specified in ASTM G1 – 90.

The appearances of first visible cracking were detected by visual observation using a magnification glass with power of x1000. The data collected for crack propagation provided the timing of first cracking and the subsequent time-dependent increase in crack width. After testing, the weight loss of bars due to corrosion were studied by cleaning, drying and weighing the reinforcement bars according to ASTM G1 – 90. Figure 3 shows samples during experimentation and measurement. The weight loss corresponded closely to that expected from current density (i_{corr}) measurements.

a) b) c) d) e)

Figure 3: a) Samples during experimentation b) sample with 0.2 mm longitudinal crack c) crack measurement d) recovering the corroded steel and e) cleaned rebar's for gravimetric weight loss measurement

3. Results and Discussions

Physical and mechanical tests on aggregates were carried out to determine their suitability for use in the study.

3.1 Results and Discussion of Material Properties

Water soluble chlorides ions in fine aggregates were found to be zero percent and 0.002 % in coarse aggregates. The percentage of chloride is less than the maximum limit of 0.03% as per BS EN 12620; 2013 and therefore acceptable for use. High water soluble chlorides in the aggregates may aggravate the threshold available in concrete and contribute to corrosion. Table 5 shows the physical properties of the aggregates used in this study.

Table 5. Physical properties of aggregates used in the study

Material	Specific gravity	% Water Absorption	% Silt content	Max. Size(mm)
FA	2.6	1.8	7.4	4.0
CA	2.6	0.3	0	20.0

As seen in Table 5, the specific gravity of all the aggregates is within the limits of 2.4–3.0 conforming to BS EN 1097-6:2013 and they influence the mix design of the concrete. The optimal concrete strength is attained when the specific gravity of coarse aggregates is higher than that of water and lower than that of cement. The water absorption of the fine aggregates is within the limits of 1%–3% in BS EN 1097-6:2013 implying a low water absorption hence being suitable for concrete works. The low water absorption in the coarse aggregates was taken into consideration in the mix design.

ASTM C117 – 17 gives an allowable limit of 10% for silt and clay content in fine aggregates for concrete production, while BS EN 12620:2013 gives an upper limit of 3% for non-harmful fines. The silt content in the fine aggregate was more than the allowable percentage of silt content; it was washed and oven-dried before use. Table 6 shows the mechanical properties of the coarse aggregates used in this study.

Table 6. Mechanical properties of coarse aggregates

Test	Result	Limit
Crushing value %	18	<45
Impact Value %	8	<45
Loss Angeles Abrasion Value %	20	30

The mechanical properties of aggregates cannot be improved but depend on the properties of the parent rock. The Aggregates Impact Value is less than 30% specified in KS EAS 18-1:2017. It, therefore, follows that the Aggregates Impact Value of all the aggregates tested were very suitable for concreting works.

The particle size distribution analysis on a representative sample, as shown in Figure 4 of the course aggregates for the work, was carried out to obtain the proportions by weight of the different sizes of coarse aggregates present. The sample is well graded with a maximum aggregate size of 20 mm. From the gradation curve, a reasonable portion falls within the gradation limits. Reasonable workability can be achieved with such aggregates without greater fines.

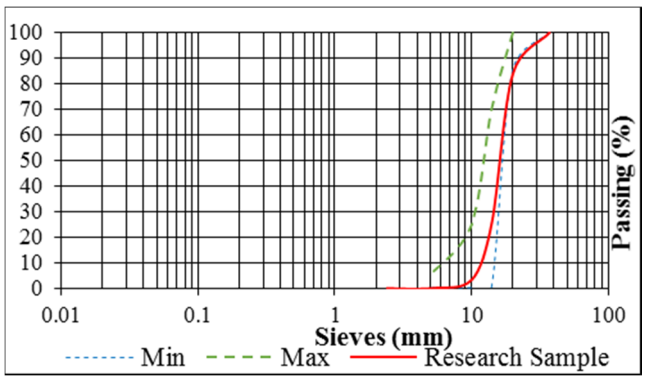

Figure 4. Gradation of Coarse aggregates

Particle size distribution analysis, as shown in Figure 4, on a representative sample of the fine aggregates for the research was carried out to obtain the proportions by weight of the different sizes of fine particles present according to BS EN 933-1:2012. The proportions were expressed as percentages by weight passing various sieve sizes conforming to BS 410. As shown in Figure 5, the fine aggregates were well graded and expected to give a well interlocked composite concrete mix.

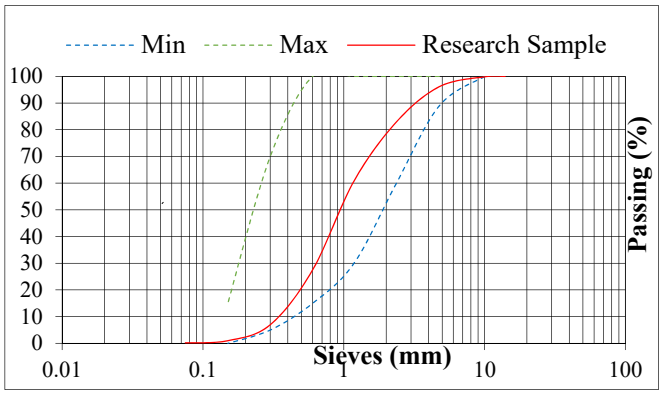

Figure 5. Gradation of fine aggregates

Table 7 shows the chemical properties of the selected Cem 1 brands in Kenya used in this study.

Table 7. Chemical composition of the cement used in the study

Test	Result			KS EAS 18-1: 2017 Requirement
	Cem A	Cem B	Cem C	
CaO%	59.86	59.11	58.82	Sum ≥ 50
SiO_2%	16.56	21.56	19.47	
SO_3%	2.02	2.78	2.03	≤ 3.5
MgO%	1.76	1.04	0.57	≤ 5
K_2O%	0.027	0.051	-	
Fe_2O_3%	2.32	3.48	1.44	
Al_2O_3	7.61	8.09	6.85	3-8
Na_2O_3%	0.054	0.018		
LOI%	0.11	0.10	4.75	≤ 5
Cl%	0.012	0.016	0.014	≤ 0.1
IR%	2.20	0.55	1.96	≤ 5

From Table 7, Cem A has the highest amount of lime(CaO) (59.86%) and Insoluble residue (2.20%), Cem B has the highest Silicon dioxide (SiO_2) (21. 56%). The increased sum of (CaO) and (SiO_2) increases compressive strength and subsequently, bond strength and critical penetration depth should not be less than 50%. Similarly, an increase in insoluble residue reduces compressive strength. All cement samples used for this work satisfied this requirement of KS EAS 18-1:2017. Cement sample B has a CaO + SiO_2 value of 80.67 % and produced the highest compressive strength of concrete (44.89 N/mm^2). SiO_2 has to be limited relative to CaO in order not to negatively affect setting time.

The ratio (CaO)/(SiO_2) contents in Cem 1 cement should be greater than 2. The restriction is to ensure that the setting of concrete is not inhibited. All the cement samples investigated fulfilled this requirement. The ratio of CaO/SiO2 in interaction with an insoluble residue of cement influences the compressive strength.

The quantity of magnesium oxide (MgO) in Cem 1 cement should not exceed 5%. All the cement samples satisfied this requirement with 1.76%, 1.04% and 0.57% for cement samples A, B and C, respectively. MgO contributes to the colour of cement and hardness of the resulting concrete. If the quantity of MgO is more than 5%, cracks will appear in concrete, which may reduce the bond strength by reducing the effective length. Cracks may subsequently increase and accelerate the critical penetration depth.

The chloride content in ordinary Portland cement should be less than 0.4%. All the cement samples in this work satisfied this requirement. Chloride content limits ensure a reduced amount available to aggravate corrosion, which in turn reduces bond strength.

Na2O, K_2O, TiO_2 and P_2O_5 in Cem 1 are considered residues and their sum is limited to 5% (Sharma, 2020). All the cement samples investigated fulfilled this requirement, with cement samples A, B and C having total residue contents of 0.55, 2.2 and 1.96%, respectively. If these values are more than 5%, efflorescence and unsightly cracking will occur, thus reducing the bond strength.

3.2 Results of fresh concrete test

The result for the slump test of the fresh concrete is shown in Figure 6. The slumps obtained are in the medium range (68-93 mm).

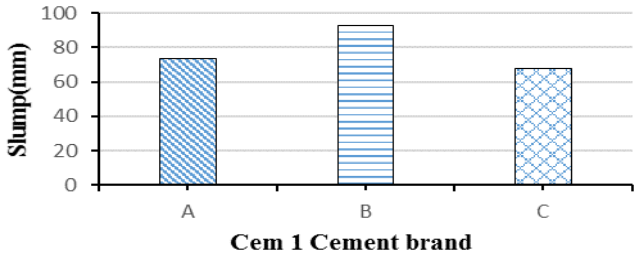

Figure 6. Slump from Cem 1 brands of cement

From Figure 6, concrete with Cem B brand of cement had the highest slump while C had the lowest slump. Workability increases with an increase in a slump and this reduces the resulting strength on concrete.

3.3 Results of Hardened Concrete

Table 8 shows the compressive, split tensile and bond strength results.

Table 8. Results of properties of hardened concrete

Cem 1 brand	Compressive strength (N/mm^2	Tensile strength (N/mm^2)	Bond strength (N/mm^2)
A	41.29	4.5	4.42
B	41.09	4.45	4.33
C	44.89	4.48	4.4

From Table 8, Figures 7, 8 and 9 are drawn to show the relationship of the hardened properties of concrete for a selected brand of cement. Figure 7 shows a bar chart of a comparative relationship of the hardened properties of concrete with a selected Cem 1 brand.

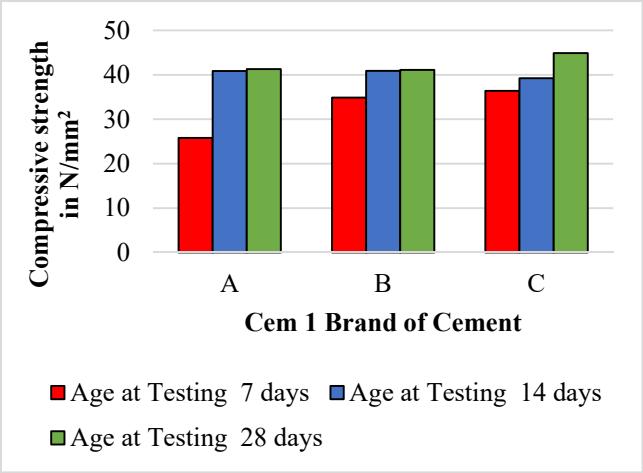

Figure 7. Bar chart of Compressive strength for selected Cem 1 Cement brand

From Figure 7, it can be noted that a choice of a brand of Cem 1 cement influences the compressive strength. As expected, Cem C with the highest CaO/SiO_2 ratio in interaction with insoluble residue had the highest compressive strength. A high compressive strength increases bond strength and affects the critical penetration depth. This result is also in line with those from Fig.3, as increase in slumps causes reduced strength, durability and permeability of concrete. The test was carried out after 27 days of curing.

Figure 8 shows a bar chart of the relationship of split tensile strength and a selected Cem 1 brand of cement as shown in Table 8.

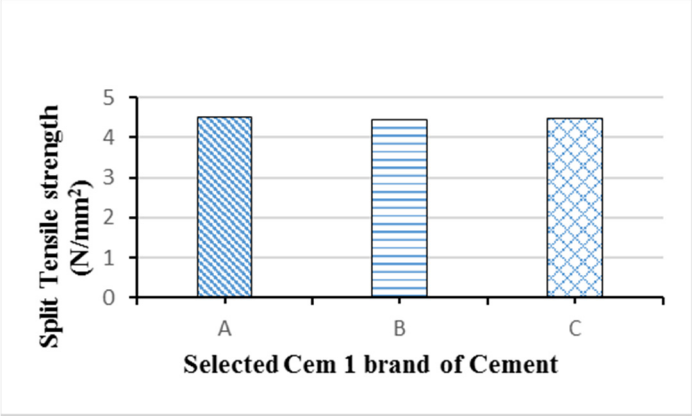

Figure 8. Bar Chart showing the relationship of split tensile strength of concrete with selected Cem 1 brands of cement

From Figure 6, it can be shown that concrete with Cem C has the highest split tensile strength. Cem C has the highest CaO/SiO_2 ratio in combination with insoluble residue and increases the compressive strength and subsequently the split tensile strength. Fig.7 shows a relationship between bond strength and a brand of Cem 1 cement.

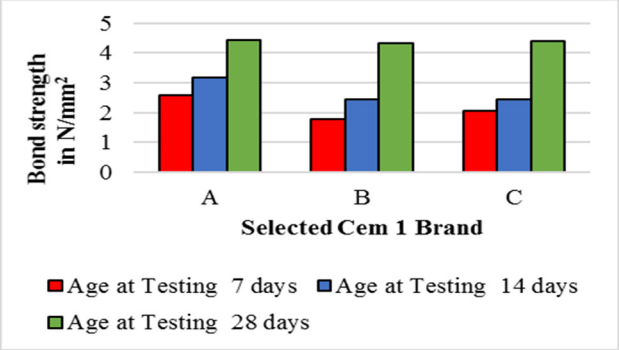

Figure 9. Relationship of bond strength and selected Cem 1 cement brand

From Figure 9, a selected Cem 1 cement brand influenced the bond strength of the reinforced concrete samples. Samples with Cem B brand of cement had the lowest chemical constituents that affect compressive strength and subsequently had the lowest bond strength as expected.

Based on the results shown in Figure 7, the choice of Cem 1 brand of cement significantly affects the bond strength and subsequently the service life of the respective structures.

Table 9 shows a statistical relationship between split tensile and bond strength in a linear regression statistical model with a 96.2 % coefficient of determination.

Table 9. Statistical relationship between tensile and bond strength

R Squire	F	Sig	Constant	b1
0.962	25.21	0.124	2.187	0.522

From Table 9, Equation 2 is proposed for this study.

$$ft = 2.187 + 0.522f_b \quad (2)$$

Where f_b is the bond strength (MPa).

3.4 Results from Accelerated Corrosion Tests

$$\Delta W=25It \quad (3)$$

Where, ΔW = calculated mass loss in grams.

I = corrosion current (amp) averages measured during accelerated corrosion (4.0,2.4 and 2.0 milliampares for concrete characteristic strength 35N/mm^2,30N/mm^2 and 25N/mm^2 respectively) and t = time (days).

$$\text{Corrosion Rate(mm/yr)}= 87.6 \text{ x } [w/(D \text{ x } A \text{ x } T)] \quad (4)$$

where W is the weight loss in milligrams measured as an average from corroded samples.

D is the density of the rebar used, g/cc, =7.8

A is the surface area of the specimen subjected to corrosion (cm^2), and =91.11

T is the duration of the test period in hours.

Table 10. The rate of corrosion of rebar from samples from different diameter samples and strengths

Concrete characteristic strength	Sample series	Rate of corrosion in mm/yr						
		Average mass of steel sample before corrosion (gms)	Average mass of steel sample after corrosion (gms)	Loss in weight (gms) measured	Loss in weight (gms) Calculated	Duration in days	Rate of corrosion mm/yr (measured)	Rate of corrosion mm/yr (calculated)
25N/mm^2	150mm diameter	371	360.4	10.6	10.7	107	0.51	0.51
	130mm diameter	371	362.3	8.7	8.7	86	0.52	0.52
	100mm diameter	371	363.2	7.8	7.6	76	0.53	0.52
30N/mm^2	150mm diameter	371	361.5	9.5	9.4	156	0.31	0.31
	130mm diameter	371	362.4	8.6	8.5	142	0.31	0.31
	100mm diameter	371	363.4	7.6	7.6	127	0.31	0.31
35N/mm^2	150mm diameter	371	361.6	9.4	9.3	186	0.26	0.26
	130mm diameter	371	362.4	8.6	8.6	172	0.26	0.26
	100mm diameter	371	363.1	7.9	7.9	158	0.26	0.26

Figure 10 shows a graph of the Relationship of the rate of corrosion and the characteristic strength of concrete derived from Table 10.

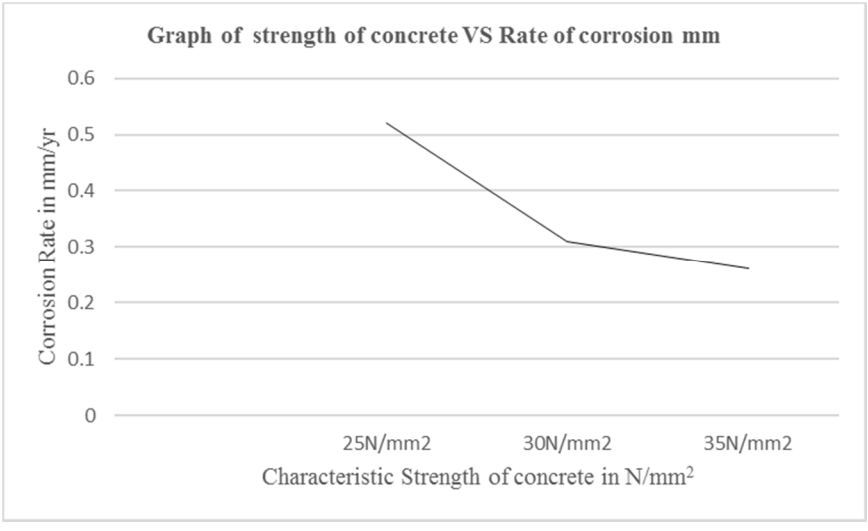

Figure 10. Relationship of the rate of corrosion vs the rate of corrosion

From Table 10 and Figure 10, it can be observed that the rate of corrosion is affected by the characteristic strength and this is attributed to the rate at which the aggressive chloride ions took to reach the rebar to enhance the onset of corrosion. It took a longest period for samples of characteristic 35N/mm^2 to corrode and result to a crack width of 0.2 mm while samples with characteristic strength 25 N/mm^2 exhibited the shortest time. It can also be observed

that concrete cover affects the duration of corrosion within the same characteristic strength of concrete but the rate of corrosion remains the same and this is because concrete of the same characteristic strength has the same electrical resistance.

It was also observed that the rate of corrosion in rebar reduced with an increase in characteristic strength. Concrete with a higher characteristic strength has a low permeability and a high inhibition of the cathodic site and the hydroxyl ion conduit from forming. Consequently, the reduction in permeability with increasing characteristic strength reduces the rate of corrosion in addition to crack initiation in concrete.

3.5 Crack Initiation (t_1)

This is the first visible crack, which was observed through a magnifying glass (x1000) and this period of time (t_1) can be referred to as time to crack initiation. t_1 depends on concrete tensile strength (f_t).

3.6 Crack Propagation (t_2)

Cracks first observed at the concrete surface through the magnifying glass were very small (width of less than 0.2mm) with lengths varying from 30mm to 300mm.Cracks width and length then increased in an inhomogeneous manner until they extended and joined together to create continuous corrosion-induced longitudinal cracking when the crack width was 0.2mm when the experiment stopped.

3.7 Time to Cracking

When the amount of corrosion products reaches the critical amount of rust products, the internal expansion stress will exceed the tensile strength of concrete and cause the cracking of the cover concrete. According to equation 11, for a constant corrosion rate, the time to cracking, t_{cr} can be given as follows:

$$t_{cr} = M^2_{crit}/2[2.59\ X10^{-6}\left(1/\alpha\right)\pi D i_{cor} \quad (5)$$

where

M_{crit} is the critical amount of corrosion products in kilograms.

α is the ratio of the molecular weight of rust to that of iron,

D is the steel diameter (cm.) and

i_{cor} is the annual mean corrosion rate ($\mu A/cm^2$).

Since corrosion rate is a function of corrosion time,using the numerical method, the time to cracking can be also calculated from equation 5.

Table 11 Based on calculated critical amount of rust products the times to cracking is obtained from equation 5. The results are summarized in Table 11. As it can be seen from the Table in column 6, the measured times to cracking are within the predicted values by the model.

Table 11. Parametric study of predicted and observed times to cracking of the research and the model

Concrete characteristic strength	Sample series X300mm length	Cover	Measured corrosion rate mm/year	Real corrosion rate mm/year	Time in years Model predicted*	Time in years Measured
25N/mm^2	100diameter	70	0.51	0.51k_p	0.153-0.319	0.215
	130mm diameter	60	0.52	0.52k_p	0.186-0.389	0.243
	150mm diameter	45	0.53	0.53k_p	0.272-0.566	0.302
30N/mm^2	100mm diameter	70	0.31	0.31k_p	0.239-0.498	0.441
	130mm diameter	60	0.31	0.31k_p	0.306-0.638	0.401
	150mm diameter	45	0.31	0.31k_p	0.374-0.778	0.359
35N/mm^2	100mm diameter	70	0.26	0.26k_p	0.285-0.594	0.525
	130mm diameter	60	0.26	0.26k_p	0.365-0.761	0.486
	150mm diameter	45	0.26	0.26k_p	0.436-0.908	0.430

**The model predicted times to cracking were calculated taking α_1 value of 1.8 for (FeO) and 3.75 for (Fe(OH)2) for corrosion product.*

From Table 11, it can be observed that the measured times to cracking are within the model predicted time.

From Table 11, Figure 11a), b) and c) are drawn showing a relationship between measured and real corrosion rate for reinforced concrete water structures.

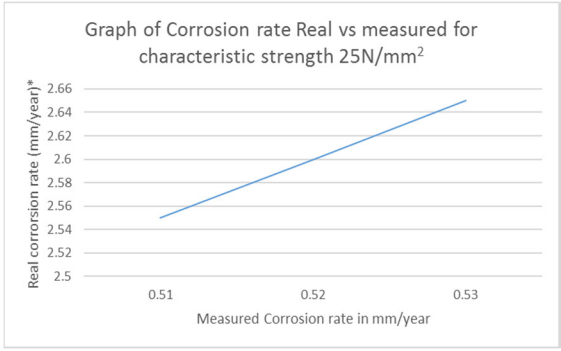

Figure 11a)

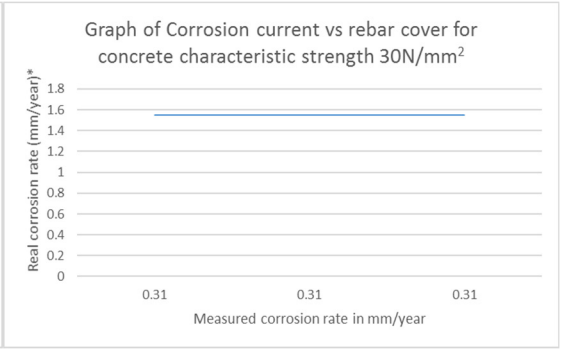

Figure 11b)

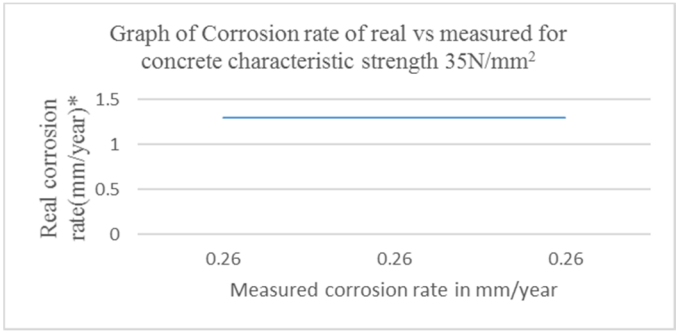

Figure 11c)

**Real corrosion rate=3k_p*

For low corrosion rates:

$$T_{2(real)} = k_p \text{ x } T_{2(exp)} \tag{6}$$

$$K_p = k_R \text{ x } \frac{i_{corr(exp)}}{i_{corr(real)}} \tag{7}$$

Where

$T_{2(real)}$ = Corrosion propagation time for real structures

k_R = Rate of loading correction factor

$i_{corr(exp)}$ = accelerated corrosion rate

$i_{corr(real)}$ = any value of selected corrosion rate

$T_{2(exp)}$ = is the measured time and can be obtained from the proposed model

If the rate of loading does not affect crack propagation, then $k_R = 1$. Empirically:

$$k_R \approx 0.95 \left[\exp\left(\frac{-0.3 i_{corr(exp)}}{i_{corr(real)}}\right) - \frac{i_{corr(exp)}}{i_{corr(real)}} + 0.3\right], k_R \geq 0.25 \tag{8}$$

4. Conclusion

A study of selected Cem 1 brands of cement intended for structural applications has been done in this research. The variation in the chemical composition of the selected brands affects the compressive, split tensile, bond strength and critical penetration depth. According to the analyses and experiments of hardened properties of the

tested samples, it was found that available Cem 1 brands of cement in the Kenyan market vary in chemical composition, and this affects the hardened properties of concrete.

It can also be deduced that the rate of corrosion in reinforced concrete increases with a reduction of concrete cover and compressive strength, and this is attributed to all the factors that affect the spilt tensile strength, which subsequently affects both properties. The relationship between the rate of corrosion from accelerated corrosion tests and real structures linear and in this can be used in the calculation of the ervice life of reinforced concrete structures.

Funding

None

Competing Interests

Sample: The authors declare that they have no known competing financial interests or personal relationships that could have appeared to influence the work reported in this paper.

Provenance and Peer Review

Not commissioned; externally double-blind peer reviewed.

Data Availability Statement

The data that support the findings of this study are available on request.

Data Sharing Statement

No additional data are available.

References

ACI 318-08. *Building Code Requirements for Structural Concrete and Commentary*. American Concrete Institute, U.S.A.

CI Committee 222. (2001). *Protection of Metals in Concrete Against Corrosion*. ACI 222R-01, American Concrete Institute, Farmington Hills, Michigan.

Alonso, C., Andrade, C., Rodriguez, J., & Diez, J. M. (1998). Factors controlling cracking of concrete affected by reinforcement corrosion. *Materials and structures*, *31*, 435-441. https://doi.org/10.1007/BF02480466

Andrade, C., Alonso, C., & Molina, F. J. (1993). Cover cracking as a function of bar corrosion: Part I-Experimental test. *Materials and structures*, *26*, 453-464. https://doi.org/10.1007/BF02472805

ASTM C117 - 17. *Standard Test Method for Materials Finer than 75-μm* (No. 200). Sieve in Mineral Aggregates by washing, ASTM International. U.S.A.

Bažant, Z. P. (1979). Physical model for steel corrosion in concrete sea structures-Application. *Journal of the structural division*, *105*(6), 1155-1166. https://doi.org/10.1061/JSDEAG.0005169

Bhargava, K., Ghosh, A. K., Mori, Y., & Ramanujam, S. (2005). Modeling of time to corrosion-induced cover cracking in reinforced concrete structures. *Cement and Concrete Research*, *35*(11), 2203-2218. https://doi.org/10.1016/j.cemconres.2005.06.007

Bhargava, K., Ghosh, A. K., Mori, Y., & Ramanujam, S. (2006). Model for cover cracking due to rebar corrosion in RC structures. *Engineering Structures*, *28*(8), 1093-1109. https://doi.org/10.1016/j.engstruct.2005.11.014

British Standard Institute. (2009). *EN 12390-5:2009. Testing hardened concrete - Part 5: Flexural strength of test specimens*.

British Standard Institute. (2009). *BS EN 12390-6:2009: Testing hardened concrete*. Tensile splitting strength of test specimens.

British Standard Institute. (2012). *BS EN 12390-1:2012: Testing hardened concrete. Shape, dimensions and other requirements for specimens and moulds*.

British Standard Institute. (2012). *BS EN 933-1:2012: The Standard for Tests for geometrical properties of aggregates - Determination of particle size distribution*.

British Standard Institute. (2013). *BS EN 12620(2013): Aggregates for concrete.*

British Standard Institute. (2013). *EN 1097-6:2013: Tests for mechanical and physical properties of aggregates - Part 6: Determination of particle density and water absorption.*

British Standard Institute. (2019). *BS EN 12390-2:2019: Testing hardened concrete Making and curing specimens for strength tests*.

Du, Y. G., Chan, A. H. C., & Clark, L. A. (2006). Finite element analysis of the effects of radial expansion of corroded reinforcement. *Computers & structures*, *84*(13-14), 917-929. https://doi.org/10.1016/j.compstruc.2006.02.012

Ejiogu, I. K., Mamza, P. A. P., Nkeonye, P. O., & Yaro, S. A. (2020). Comparison of aci, is and doe methods of concrete mix design. *Nigerian Journal of Engineering*, *27*(1), 68-68.

Ghods, P., Isgor, O. B., Bensebaa, F., & Kingston, D. (2012). Angle-resolved XPS study of carbon steel passivity and chloride-induced depassivation in simulated concrete pore solution. *Corrosion Science*, *58*, 159-167. https://doi.org/10.1016/j.corsci.2012.01.019

Kenya Bureau of Standards, KS EAS 18-1: 2017-Cement Part 1: Composition, Specification and Conformity Criteria for Common Cements. Kenya Bureau of Standards, Nairobi, 2017.

Kiani, K. (2002). *Study of reinforcement corrosion in RC structures via reproducing kernel particle method* (Doctoral dissertation, M. Sc. Thesis. Tehran, Sharif University of Technology).

Li C.Q., Melchers R. E., & Zheng, J. J. (2006). Analytical model for corrosion-induced crack width in reinforced concrete structures. *ACI Struct J, 103*(4), 479-487. https://doi.org/10.14359/16423

Liu, Y., & Weyers, R. E. (1998). Modelling the time to corrosion in cracking in chloride contaminated reinforced concrete structures. *ACI Mat. J, 95*, 675-681. https://doi.org/10.14359/410

Lundgren, K. (2002). Modeling the effect of corrosion on bond in reinforced concrete. *Mag. Concr. Res., 54*, 165-173. https://doi.org/10.1680/macr.2002.54.3.165

Molina, F. J., Alonso, C., & Andrade, C. (1993). Cover cracking as a function of rebar corrosion: Part 2 - Numerical model. *Mater and Struct, 26*, 532-548. https://doi.org/10.1007/BF02472864

Morinaga, S. (1989). Prediction of Service Lives of Reinforced Concrete Buildings based on Rate of Corrosion of Reinforcing Steel. *Special report of the Institute of Technology*, Japan, Skimiza Corporation.

Palanisamy, G. (2019). Corrosion Inhibitors. *IntechOpen*. http://dx.doi.org/10.5772/intechopen.80542.

Shodja, H. M., Kiani, K., & Hashemian, A. (2010). A model for the evolution of concrete deterioration due to reinforcement corrosion. *Mathematical and Computer Modelling*, *52*(9-10), 1403-1422. https://doi.org/10.1016/j.mcm.2010.05.023